

# Interictal epileptiform discharges shape large-scale intercortical communication

Prawesh Dahal,<sup>1</sup> Naureen Ghani,<sup>2,\*</sup> Adeen Flinker,<sup>3,4</sup> Patricia Dugan,<sup>3,4</sup> Daniel Friedman,<sup>3,4</sup> Werner Doyle,<sup>4,5</sup> Orrin Devinsky,<sup>3,4</sup> Dion Khodagholy<sup>1</sup> and Jennifer N. Gelin<sup>2,6</sup>

Dynamic interactions between remote but functionally specialized brain regions enable complex information processing. This intercortical communication is disrupted in the neural networks of patients with focal epilepsy, and epileptic activity can exert widespread effects within the brain. Using large-scale human intracranial electroencephalography recordings, we show that interictal epileptiform discharges (IEDs) are significantly coupled with spindles in discrete, individualized brain regions outside of the epileptic network. We found that a substantial proportion of these localized spindles travel across the cortical surface. Brain regions that participate in this IED-driven oscillatory coupling express spindles that have a broader spatial extent and higher tendency to propagate than spindles occurring in uncoupled regions. These altered spatiotemporal oscillatory properties identify areas that are shaped by epileptic activity independent of IED or seizure detection. Our findings suggest that IED-spindle coupling may be an important mechanism of interictal global network dysfunction that could be targeted to prevent disruption of normal neural activity.

- 1 Department of Electrical Engineering, Columbia University, New York, NY, 10027, USA
- 2 Institute for Genomic Medicine, Columbia University Medical Center, New York, NY, 10032, USA
- 3 Department of Neurology, NYU Langone, New York, NY, 10016, USA
- 4 Comprehensive Epilepsy Center, NYU Langone, New York, NY, 10016, USA
- 5 Department of Neurosurgery, NYU Langone, New York, NY, 10016, USA
- 6 Department of Neurology, Columbia University Medical Center, New York, NY, 10032, USA

\*Present address: Department of Computer Science, University College London, Gower Street, London WC1E 6EA, UK

Correspondence to: Jennifer N. Gelin  
Institute for Genomic Medicine, Columbia University Medical Center, New York, NY,  
10032, USA  
E-mail: jng2146@cumc.columbia.edu

Correspondence may also be addressed to: Dion Khodagholy  
Department of Electrical Engineering, Columbia University, New York, NY, 10027,  
USA  
E-mail: dk2955@columbia.edu

**Keywords:** epilepsy; oscillation; interictal epileptiform discharge; sleep spindle; intercortical

**Abbreviations:** IED = interictal epileptiform discharge; iEEG = intracranial electroencephalography; PGD = phase gradient directionality

## Introduction

Co-ordinated oscillatory activity between brain regions facilitates neuronal communication and mediates diverse brain processes. These intercortical interactions establish temporally specific effective connectivity, thereby regulating information flow (Fries, 2005; Buzsaki and Schomburg, 2015) and promoting long-term plasticity (Benchenane *et al.*, 2010; Igarashi *et al.*, 2014).

Interictal epileptiform discharges (IEDs) and seizures are pathological hypersynchronous patterns of brain activity that are localized in patients with focal epilepsy (Rosenow and Luders, 2001; Bartolomei *et al.*, 2017). However, neuropsychological, structural and functional indicators suggest that these patients' brains demonstrate abnormalities that extend beyond the region from which IEDs and seizures can be recorded (epileptic network) (Bettus *et al.*, 2011; Englot *et al.*, 2016; Lagarde *et al.*, 2018; Tong *et al.*, 2019). The mechanisms by which epileptic activity interacts with and shapes these large-scale neural networks in the human brain remain mostly unknown and have implications for associated neuropsychiatric dysfunction and progression of focal epilepsy.

Non-rapid eye movement (NREM) sleep is a critical brain state for long-range intercortical communication, and strongly contributes to consolidation of memory within distributed cortical networks (Diekelmann and Born, 2010). A key electrophysiological marker of this brain state is the thalamocortical spindle (9–16 Hz) (Steriade *et al.*, 1993; Diekelmann and Born, 2010). Evidence implicates spindles in regional information processing: (i) brain area specific changes in spindle properties occur after learning (Gais *et al.*, 2002); (ii) artificially increasing the coupling of spindles with other patterned oscillations improves memory (Maingret *et al.*, 2016); and (iii) neural spiking sequences from waking experience are replayed during spindles (Johnson *et al.*, 2010; Sawangjit *et al.*, 2018). In parallel, IED frequency is often increased in NREM sleep, and can be influenced by the slow oscillation (Frauscher *et al.*, 2015) as well as sleep phase (Ujma *et al.*, 2017). In an animal model, hippocampal IEDs can evoke spindles in an anatomically remote but synaptically connected cortical region, and this pathological coupling correlates with impaired memory (Gelinas *et al.*, 2016). Pilot data suggest that similar coupling occurs in patients with epilepsy (Gelinas *et al.*, 2016).

We hypothesized that IEDs in patients with focal epilepsy can couple with spindles, creating pathological functional connectivity that enables epileptic activity to exert influence beyond the epileptic network. To test this hypothesis, we analysed intracranial EEG (iEEG) data from patients with focal epilepsy who required large-scale electrophysiological monitoring to localize seizures during clinical work-up for epilepsy surgery. We demonstrate that IEDs occurring

throughout the cortex can reliably induce spindles, generating individualized patterns of IED-spindle coupling. Regions that respond to IEDs with expression of spindles are distinct from the epileptic network, and display altered oscillatory spatial extent and propagation. These IED-driven, spatiotemporally-specific patterns of abnormally coordinated brain activity could provide a mechanism for large-scale disruption of neural network function in focal epilepsy, potentially contributing to impairment of processes that heavily rely upon intercortical communication, such as cognition and memory.

## Materials and methods

### Subjects

We analysed iEEG recordings from 10 patients with focal epilepsy who underwent clinical electrode placement as part of the work-up for epilepsy surgery. Gathering and analysis of these data were approved by the Institutional Review Board at New York University Langone Medical Center (NYULMC), and all data collection occurred at this institution. Informed written consent was obtained from all patients according to the Declaration of Helsinki. Each patient had a configuration of electrodes implanted based on clinical need, including subdural grids and strips, as well as depth electrodes. Patients with focal epilepsy with continuous high quality iEEG recordings that included at least one 8 × 8 subdural grid (1 cm electrode spacing, centre to centre) in the absence of major cortical lesions were eligible for analysis. The majority of patients had normal neuroimaging; when lesions were subsequently resected they were pathologically identified as focal cortical dysplasia or low-grade tumour. All patients had a similar number of electrodes available for analysis (Supplementary Table 1). Recordings included waking and sleep epochs; no task-related data were analysed.

### Clinical reports

We obtained the clinical iEEG reports for each patient's hospital admission. Each report detailed the date, time, semiology, onset and propagation of seizures, as well as clinical localization of IEDs. Data were clinically interpreted using a combination of referential montage (referenced to epidural electrodes) and bipolar montage (based on pairs of neighbouring electrodes). Epochs of iEEG data corresponding to these seizures were identified for further analysis.

### Intracranial EEG data preprocessing and detections

Epochs of sleep were identified by immobility (lack of change in a motion vector extracted from synchronized video files) in concert with increased delta/gamma frequency ratio in the iEEG spectrogram. Referential data were imported into MATLAB and resampled from 512 to 1250 Hz for compatibility with previously validated analytical toolboxes. IED detection was performed on all electrodes, using a combination

of frequency, amplitude and duration parameters: (i) bandpass filtering at 25–80 Hz and signal rectification; (ii) detection of events where the filtered envelope was >3 times above baseline; (iii) elimination of events where the unfiltered envelope was <3 times above baseline; and (iv) elimination of IEDs occurring within 500 ms of another IED to prevent over-correlation due to a run of IEDs (Gélinas *et al.*, 2016). Detected IEDs had waveforms consistent with typical interictal spikes and/or sharp waves, and were variably associated with an aftergoing slow wave (Supplementary Fig. 1). Spindle detection was performed based on wavelet-derived power and duration parameters. A ratio of normalized autoregressive wavelet-based  $P_{AR}$  was first calculated based on the following equation:

$$P_{AR} = \frac{P_{spi} - (P_{low} + P_{high})}{P_{spi} + (P_{low} + P_{high})} \quad (1)$$

where spindle band power ( $P_{spi}$ ) was based on 10–20 Hz, low band power was based on 2–8 Hz ( $P_{low}$ ), and high band power was based on 25–40 Hz ( $P_{high}$ ). Spindle events were identified when the ratio crossed zero and was >0.1 for a minimum of 300 ms and a maximum of 3 s. We detected both fast (13–15 Hz) and slow (9–12 Hz) spindles using this approach. All detections were visually inspected for accuracy for each recording session.

## Intracranial EEG electrode localization

Localization of intracranial electrodes was performed based on reconstruction of subject-specific pial surfaces, co-registration of pre- and post-implant MRI images, a combination of manual and automatic localization of electrodes, and subsequent co-registration to a standard template brain (Yang *et al.*, 2012). MNI coordinates and the gyral location of electrodes (determined based on cortical parcellation using the Desikan-Killiany atlas) (Desikan *et al.*, 2006) were used for across-subject localization comparisons. For visualization of group data, electrode MNI coordinates from patients with right hemisphere electrodes were converted to corresponding left hemisphere coordinates.

## Intracranial EEG spatiotemporal analysis

We used a combination of freely available, online MATLAB toolboxes (Freely Moving Animal Toolbox; <http://fmtoolbox.sourceforge.net>; Chronux; <http://chronux.org>) and custom MATLAB code. Cross-correlograms, calculated using a modified convolution method (Stark and Abeles, 2009), enabled temporal correlation between detected events. Spindles were designated as coupled to an IED if they occurred within 1 s after the IED. Power was extracted using wavelet transformation (Gabor). Spatial extent of oscillations was determined by two methods, which provided complementary results: (i) cross-correlation of detected events and identification of electrodes with significant zero time lag values; and (ii) determination of wavelet-based coherence at the time of detected events.

## Intracranial EEG phase analysis

### Initial processing

To extract spindle phase, we first applied a third order 10–15 Hz bandpass Butterworth filter to the local field potential recordings from all the electrodes within the  $8 \times 8$  subdural grid at the time of each detected spindle (spindle trial). Filtered data were downsampled to 125 Hz and Hilbert transform was performed to extract the instantaneous phase of the spindles. We compared this method to cycle-by-cycle time domain analysis (Cole and Voytek, 2018). The peaks, troughs and flank midpoints in individual spindle cycles were identified and a phase time series was estimated by interpolating between the theoretical phases at these points. We obtained similar results in the instantaneous phases and their gradients extracted using these two methods (Supplementary Fig. 4D and E). We did not incorporate electrodes of subdural strips or depths in this analysis, due to their inconsistent geometry relative to adjacent electrodes.

### Calculation of phase gradient directionality

We computed the phase gradient directionality (PGD) to quantitatively assess whether spindles behaved as travelling waves across the cortex. PGD is a measure of the alignment of phase gradients of oscillations over space (Rubino *et al.*, 2006). If the PGD exceeds a threshold value, the oscillations in that space exhibit wave-like travelling for which the direction can be estimated. We sought to determine PGD values across a spatial extent that consistently demonstrated amplitude coherent spindles to minimize spurious phase values that could be elicited by filtering. Across patients, this spatial extent was found to be a cluster of  $3 \times 3$  electrodes (Supplementary Fig. 4). We verified expected variations in PGD based on cluster size, with smaller clusters exhibiting higher PGD values (consistent with phase gradients that are highly aligned over a short distance), and larger clusters exhibiting lower PGD values (consistent with the primarily spatially localized nature of the oscillations) (Supplementary Fig. 5). Therefore, we characterized systematic variations in the spindle phase across a region of nine electrodes organized in a  $3 \times 3$  cluster. By sliding this window over the entire  $8 \times 8$  electrode space, we obtained a total of 36 oscillation clusters for each patient grid. For each cluster and its corresponding number of spindle trials, the instantaneous phase at the start time point of the spindle was extracted. Having obtained a spatial array of instantaneous phase values, we computed the PGD as:

$$PGD = \frac{\|\nabla\varphi\|}{\|\nabla\varphi\|} \quad (2)$$

If a cluster contained noisy or missing electrodes, the instantaneous phase for those electrodes was interpolated using neighbouring phase values. We identified the spindle trials that demonstrated significant PGD values ( $PGD > \text{threshold}$ ) and estimated the propagation directions across those trials by calculating the angle between the average horizontal and vertical phase gradients of that cluster.

### Determination of threshold for phase gradient directionality significance

For each patient's subdural grid, we computed a single threshold to determine the significant PGD values in all oscillation

clusters. We identified five test clusters located on the corners and centre regions of the grid. For each cluster and spindle trial, we shuffled the phase values across the  $3 \times 3$  region for 500 iterations per spindle trial and computed the median PGD for each iteration. The 95th percentile of this shuffled phase distribution signified the PGD threshold for that cluster. We averaged the threshold values across the five test clusters to obtain the final PGD threshold for each patient's grid electrodes. PGD values that exceeded this threshold in each  $3 \times 3$  cluster were classified as significant.

### Consistency of directional travel

For significant PGD values, we calculated the consistency of directional travel [i.e. the degree to which spindles travelled in preferred direction(s)]. Because the preferred travelling direction of a population of spindle events is not necessarily unimodal, we convolved the histogram of the spindle direction angles with a finite Gaussian window and estimated the 95th per cent confidence intervals using a Poisson distribution (Stark and Abeles, 2009). The maximum of the angle bins that surpassed the upper bound of the confidence interval represented preferred direction(s) of spindle travelling in each cluster. To determine clusters that expressed both a high proportion of travelling spindles and highly preferred direction(s) of travel, we calculated a modulation index (MI) based on the histogram of spindle propagation angles as follows:

$$MI = \frac{hist_{max} - hist_{mean}}{hist_{max} + hist_{mean}} \quad (3)$$

For each patient, we determined the histogram mean per cluster (local mean), and the mean of all cluster histograms combined (global mean). When the local and global means differed by more than an order of magnitude, the global mean was used to calculate the modulation index; otherwise the local mean was used. This approach enabled identification of the region with the highest number of travelling spindles with consistent direction of travel regardless of the variability in this property across the grid.

### Statistical analysis

Differences between groups were calculated using non-parametric ranksum (Wilcoxon) or ANOVA (Kruskal-Wallis with Bonferroni correction) depending on the nature of the data analysed. Probability distributions were compared using two-sample Kolmogorov-Smirnov tests. Correlations were calculated using a correlation coefficient matrix based on the covariance of input variables. Error bars represent standard error of the mean (SEM). Significance level was  $P < 0.05$ .

### Data availability

The authors confirm that the data supporting the findings of this study are available within the article [and/or] its Supplementary material. Additional data are available from the corresponding author, upon reasonable request.

## Results

### Interictal epileptiform discharges induce spindles in patients with focal epilepsy

To explore the influence of IEDs on large-scale cortical networks, we analysed sleep iEEG data from patients with implanted subdural grid arrays combined with subdural strips and depth electrodes to localize seizure foci before resective surgery. We first detected and localized electrodes expressing IEDs for each patient (IED electrodes; Supplementary Fig. 1) and identified co-occurring activity patterns across all other brain regions. IEDs were observed to propagate to areas within the epileptic network (Supplementary Fig. 1). In accordance with previous results (Gelinias *et al.*, 2016), some electrodes displayed an increase in spindle power (9–16 Hz) within 1 s of IED occurrence, whereas others showed no change in any power band (Fig. 1A). We hypothesized that this IED-spindle coupling reflects a pathological connectivity that enables epileptic activity to disrupt function beyond the network of IED and seizure propagation.

To test this hypothesis, we quantified and characterized the interaction between IEDs and spindles across the full spatial extent of recorded brain regions. Cross-correlation of detected IED and spindle events revealed a subset of electrodes with significant temporal interaction between these neural patterns [spindle (SPI)-coupled electrodes] (Fig. 1B and C). Coupled spindles were initiated following IEDs at a mean latency of  $0.51 \pm 0.005$  s. The strength of IED-spindle coupling was defined as the occurrence of spindles exceeding the 95th percentile of cross-correlation within 1 s after IED occurrence. IEDs located in diverse brain regions demonstrated spindle coupling, and coupled spindles were similarly expressed in numerous areas (Fig. 1D and Supplementary Fig. 1D). Nearly all IED electrodes could generate spindles, but the proportion of electrodes expressing spindles temporally coupled to IEDs ranged from 15–67% across patients (Supplementary Fig. 2).

### Medium and long-range connections are implicated in IED-spindle coupling

We then investigated the anatomical distribution of IED-spindle coupling by localizing each IED and coupled spindle electrode to parcellated cortical areas (Desikan *et al.*, 2006). IEDs occurring in each lobe could induce spindles, with temporal lobe IEDs (within lateral temporal and limbic cortex) inducing the greatest number of coupled responses (Fig. 2A). Lateral temporal and frontal brain regions most commonly expressed spindle coupling

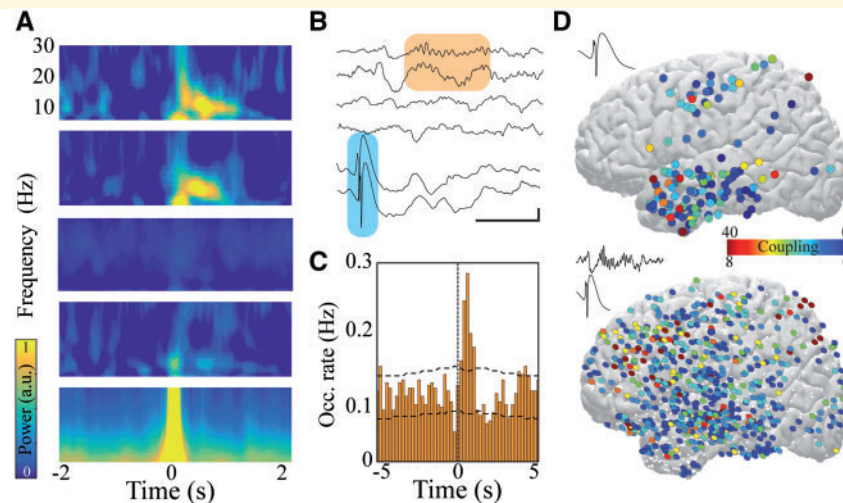


**Figure 1** IEDs induce spindles in patients with focal epilepsy. **(A)** IED trigger-averaged spectrograms derived from different electrodes reveal distinct patterns of activity: coupled spindle (*top two panels*), no change (*middle two panels*), and temporally locked IED (*bottom*). **(B)** Sample raw traces of detected IEDs (shaded blue box) and coupled cortical spindles (shaded orange box). Scale bar = 1 s, 200  $\mu$ V. **(C)** Sample cross-correlogram demonstrating significant IED-spindle coupling. IED occurrence times served as reference (time = 0, vertical dashed line) and horizontal dashed lines represent 95% confidence intervals. **(D)** Anatomical location of electrodes expressing IEDs that couple to spindles across all patients (*top*) and anatomical location of electrodes expressing spindles that are coupled to IEDs across all patients (*bottom*) projected onto lateral cortical surface (left hemisphere view; right hemisphere locations converted to left for display purposes). Colour represents number of significant IED-spindle coupling interactions per electrode location across patients. White dots show electrode locations that do not express IED-spindle coupling.

(Fig. 2B). Because IEDs were more common in the temporal lobe compared to other areas, we also estimated IED induction and SPI response potency by normalizing based on the number of electrodes capable of expressing IEDs or spindles, respectively in each brain region. This normalization revealed similar potency across lobes, with the exception of the occipital lobe, which was less likely to participate in IED-spindle coupling (Supplementary Fig. 2).

To gain insight into the anatomical substrate of IED-spindle coupling, we examined the pairs of IED-generating and SPI-coupled brain regions. A pair was identified if IEDs in a parcellated brain region resulted in a significant (>95th percentile) cross-correlation with spindles in a brain region (Fig. 2C). Most SPI-coupled electrodes did not have detectable IEDs ( $90.2 \pm 0.04\%$ ); only 7.6% of pairs were within the same parcellated brain region. IED-SPI pairs typically spanned more than one lobe (Fig. 2D), with the exception of frontal lobe IEDs, which tended to couple with other frontal cortical regions. Across all patients, the average distance between IED-SPI coupled electrodes was  $6.2 \pm 0.7$  cm (Fig. 2E), suggesting that this pathologic coordinated brain activity often spans medium-to-long distances, rather than remaining a local network phenomenon. Anatomically and temporally separate populations of IEDs could produce distinct IED-spindle coupling patterns within an individual patient (Supplementary Fig. 2), establishing the regional specificity of these interactions.

## Brain regions that demonstrate spindles coupled to interictal epileptiform discharges are outside the ictal network

We next examined the relationship between IEDs, IED-coupled spindles, and seizure activity. Electrodes were classified into five zones: seizure onset (earliest change from iEEG baseline), initial propagation (recruitment to ictal discharge within  $\leq 1$  s), middle propagation (recruitment within  $\leq 5$  s), late propagation zone (recruitment within  $\leq 30$  s) (de Curtis and Avoli, 2015), and unrecruited zone. The degree of co-localization between IEDs and seizure onset zone was highly variable across patients, but brain regions expressing IED-coupled spindles were consistently unlikely to participate in the initial stages of ictal activity (Fig. 3A–C). These areas were also relatively resistant to recruitment into seizure propagation (Fig. 3D), and were located an average of  $6.1 \pm 1.8$  cm from the seizure onset centre (Fig. 3E). Thus, the network interactions established through IED-spindle coupling are distinct from the ictal network.

## IED-spindle coupling is associated with broader spindle spatial extent across the cortical surface

We investigated whether the IED-coupled spindles exhibited different oscillation characteristics than spontaneous

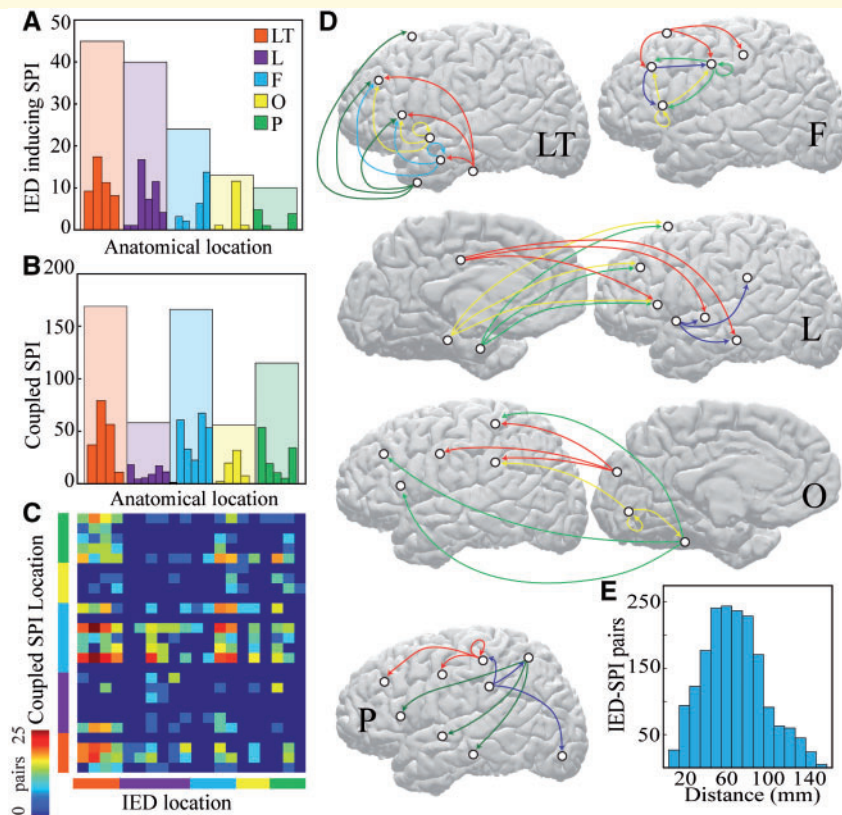


**Figure 2** Medium and long-range connections are implicated in IED-spindle coupling. **(A)** Number of electrodes expressing IEDs that couple to spindles across all patients divided by anatomical lobe. **(B)** Number of electrodes expressing spindles that are coupled to IEDs across all patients divided by lobe. **(C)** Number of IED-spindle pairs per brain region; lobes colour-coded as in **A** and **B**. Warmer colours indicate more pairs; ordered list of individual brain regions is in Supplementary Table 2. **(D)** Schematics showing the most prominent IED-spindle anatomical pairings across patients for each brain region expressing IEDs, separated by lobe and projected onto lateral and medial cortical surfaces (left hemisphere view; right hemisphere locations converted to left for display purposes). Origin of arrow indicates location of IED electrode; destination indicates location of coupled SPI electrode. White circles show location of each brain region and colours separate pairings of individual IED electrode locations. **(E)** Histogram of average distance between pairs of electrodes that interact via IED-spindle coupling. F = frontal; L = limbic; LT = lateral temporal; O = occipital; P = parietal; SPI = spindle.

spindles. The trigger-averaged spectrograms of coupled and uncoupled spindles were indistinguishable. Coupled spindles were marginally longer, higher amplitude, and lower frequency, though differences were not significant across all patients (Supplementary Fig. 3). Therefore, the temporal and morphological characteristics do not permit separation of IED-coupled and spontaneous spindles.

Spindles are commonly regional events, with restricted spatial distribution across cortex (Dehghani *et al.*, 2010; Andrillon *et al.*, 2011; Halassa *et al.*, 2011; Nir *et al.*, 2011). The broad and contiguous intracranial electrode coverage of brain regions allowed us to investigate spatial properties of IED-coupled spindles. Spindle waveform spatial extent was non-uniformly distributed across cortex (Fig. 4A and B). To quantify spatial extent, we used two complementary approaches: spindle cross-correlation and spindle band coherence (Supplementary Fig. 4). In each case, values were calculated for each pair of electrodes, and the amount of significant correlation or coherence

resulting from each comparison was summated to provide an overall indication of spatial extent for each electrode. These approaches gave consistent locations of maximal extent for each patient (Supplementary Fig. 4). This location varied considerably between patients (Fig. 4C), supporting a patient-specific factor driving spindle spatial extent variability. Most patients had significant correlation between the spatial extent of spindles in a region and the degree to which this region expressed spindles coupled to IEDs (Fig. 4D and E). Together, these results suggest that IEDs may regionally modify cortical networks to enable broad expression of local oscillations.

## Spindles travel across the cortical surface

Increased oscillatory spatial extent can be produced by a larger area expressing synchronous oscillations or by an enhanced capacity for oscillation propagation. We used

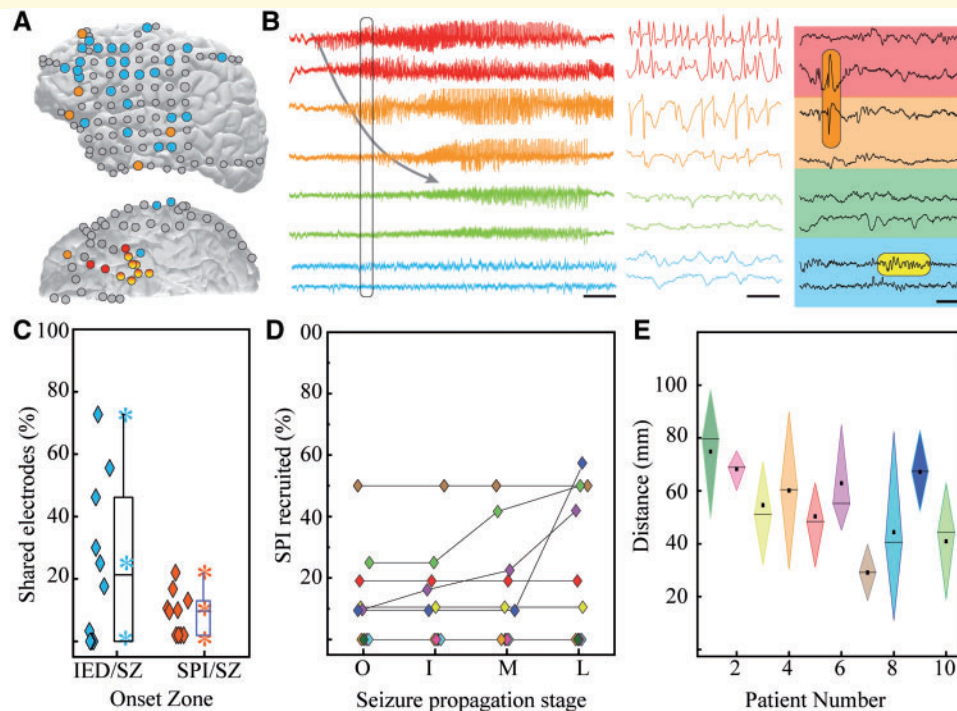


**Figure 3** Brain regions that demonstrate spindles coupled to IEDs are located outside of the ictal network. **(A)** Sample patient brain (lateral and inferior views) displaying localization of seizure onset zone (red), IED foci (orange), and regions with spindles coupled to IEDs (blue). **(B)** Raw compressed (left, scale bar = 5 s) and expanded (middle, from section of left panel defined by black box, scale bar = 125 ms) traces revealing the onset and propagation of ictal activity from electrodes in the seizure onset zone (red), middle propagation zone (orange), and late propagation zone (green). Traces from the IED-spindle coupling zone (blue) are not recruited into the ictal rhythm. Right panel shows interictal activity from these same electrodes, highlighting an IED (orange shaded box) and coupled spindle (yellow shaded box; scale bar = 200 ms) during NREM sleep. **(C)** Percentage of overlap between electrodes across patients constituting the seizure onset zone and those expressing IEDs (blue) as well as those expressing IED-coupled spindles (orange). Box shows 25th, median and 75th percentiles; stars show range and mean. Diamonds are individual data points for each patient. **(D)** Percentage of total electrodes expressing IED-coupled spindles that are recruited into successive stages of ictal activity (colours represent individual patients). I = initial propagation; L = late propagation; M = middle propagation; O = onset. **(E)** Measures of centrality and dispersion for distance between electrodes expressing IED-coupled spindles and centroid of seizure onset zone (diamond shows 25th, median, and 75th percentiles; square is mean). SZ = seizure.

PGD, which measures the alignment of phase gradients between neural oscillations (Rubino *et al.*, 2006; Zhang *et al.*, 2018), to investigate these mechanistic possibilities. We empirically defined the spatial geometry over which to probe the PGD as the largest symmetrical electrode grid that consistently displayed simultaneous increases in spindle band power (cluster of  $3 \times 3$  electrodes) (Supplementary Figs. 4 and 5). By calculating the PGD for each overlapping electrode cluster contained within the  $8 \times 8$  iEEG subdural grid implanted in each patient, we determined whether spindles were significantly propagating in a given region by comparing to a distribution of shuffled phases. Spindles ( $59.3 \pm 1.4\%$ ) had significant PGD values, indicating that they travelled across cortex (Fig. 5A and B and Supplementary Fig. 5). Traveling spindles variably had preferred direction(s) of travel (16% no preferred direction; 27% one preferred direction; 57% two preferred directions; 0%  $>2$  preferred directions) (Fig. 5C and E). We derived a measure to jointly reflect proportion of spindles with significant travelling and strength of directional travel

(modulation index; Fig. 5C and D). The modulation index was calculated for each electrode cluster, and it displayed spatial variation across each patient's subdural grid (Fig. 5D), indicating that spindles exhibited maximal directional propagation in specific regions that overlapped with the zone expressing spindles coupled to the patient's IEDs (Fig. 5F).

### Spindle spatial extent and travelling predict brain regions influenced by IEDs

Electrodes with the largest spatial extent of spindles and highest propensity for spindle propagation were significantly co-localized (Fig. 6A and Supplementary Fig. 6), suggesting that enhanced travelling could account for the broad spatial coverage. Given the overlap of these properties with expression of IED-induced spindles, we hypothesized that maximal spindle spatial extent and travelling could predict brain

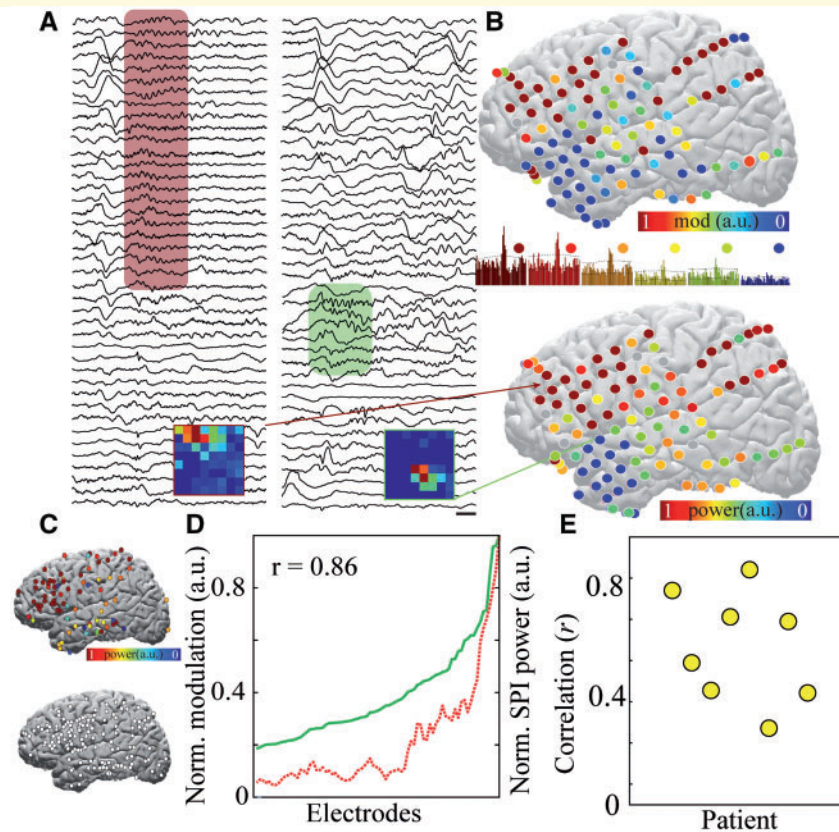


**Figure 4** IED-spindle coupling is associated with broader spindle spatial extent across the cortical surface. **(A)** Sample raw traces from 41 electrodes in a sample patient demonstrating a spatially extensive spindle (red shaded box, left) and spatially restricted spindle (green shaded box, right). Scale bar = 250 ms. Insets show the amount of spindle-spindle cross-correlation across the subdural grid using a reference electrode from the spatially extensive and restricted regions, respectively; warmer colours indicate higher zero-bin significant cross-correlation. **(B)** Comparison of electrode locations demonstrating spindles highly coupled with IEDs (top, warmer colours) and electrode locations with broad spindle spatial extent (bottom, warmer colours) from a sample patient. IED-spindle cross-correlograms with a range of significant correlations corresponding to electrode colours (middle; 10-s duration). **(C)** Normalized spindle spatial extent for all spindle electrodes (top) and spatially extensive spindle electrodes only (top 50th percentile, bottom) summated across patients and plotted on lateral cortical surface, revealing no anatomical preference for spindle spatial extent and existence of spatially extensive spindles in all lobes. **(D)** Significance of IED-spindle coupling (red) and spindle spatial extent (green) are highly correlated across electrodes for patient visualized in **A** and **B**. **(E)** Correlation between IED-spindle coupling and spindle spatial extent for all patients with > 20 significant IED-spindle pairs,  $n = 8$ .

regions influenced by IEDs. Using a predictor based on the intersection between spatial extent and propensity to travel, we found that  $81.7 \pm 0.08\%$  electrodes with significant IED-spindle coupling could be accurately predicted (Fig. 6B and C). Thus, IED-induced spindles are associated with regionally enhanced spatial extent and travelling.

## Discussion

We demonstrate that IEDs functionally interact with diverse and remote cortical regions in the human brain via induction of coupled spindles. Anatomical patterns of IED-spindle coupling are patient-specific, but consistently localized outside of the seizure onset zone. Further, spindles in brain regions targeted by IEDs have larger spatial extent and higher tendency to propagate compared to spindles in

regions unaffected by IEDs. These altered spindle properties predict brain regions distinct from the epileptic network that express neural activity patterns coordinated with IEDs, reflecting interictal network dysfunction that could possibly contribute to cognitive co-morbidities and disease progression.

We found IED-induced spindles in each patient of our cohort, suggesting that it represents a conserved reaction to epileptiform activity in cortical networks. Spindles can be induced by synchronous synaptic input to cortical circuits, as occurs in response to physiological oscillations (for instance, hippocampal sharp wave ripples) (Siapas and Wilson, 1998; Wierzynski *et al.*, 2009), as well as exogenous electrical or magnetic stimulation (Massimini *et al.*, 2007; Vyazovskiy *et al.*, 2009). The hypersynchronous neural firing associated with an IED likely generates a similar effect in cortical tissue (Bragin *et al.*, 1999), resulting in

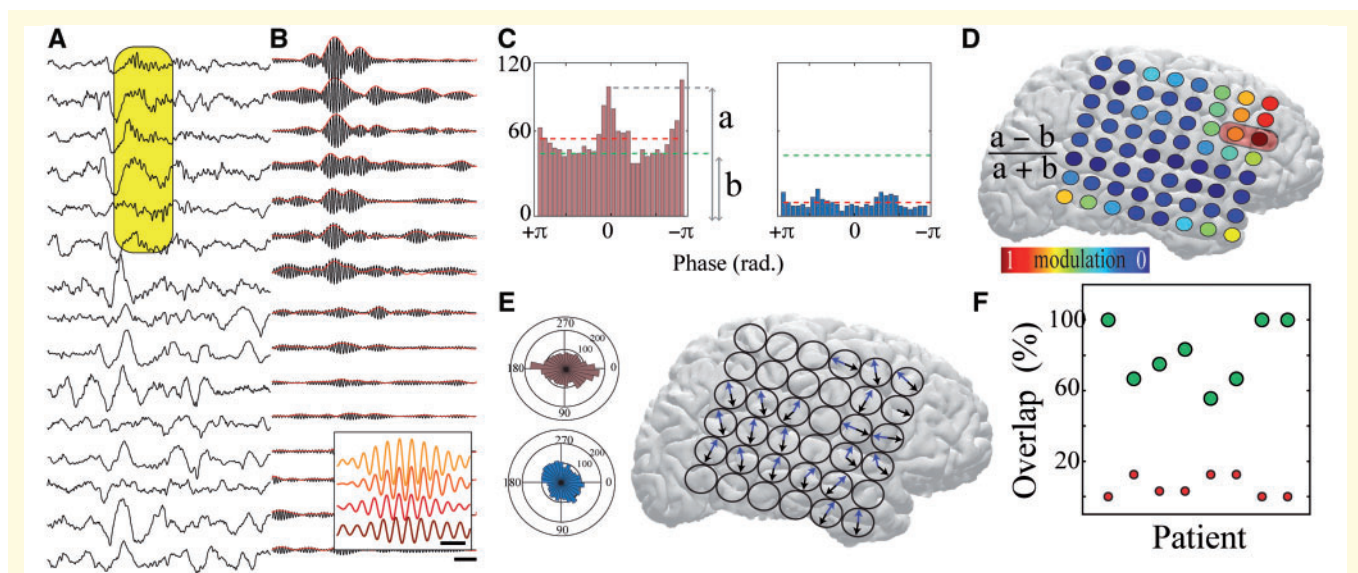


**Figure 5** Localized spindles travel across the cortical surface in regions with IED-spindle coupling. **(A)** Sample raw traces from 15 electrodes of a subdural grid revealing a spatially localized propagating spindle (shaded yellow box; scale bar = 250 ms). **(B)** Traces from **(A)** filtered at spindle band (10–15 Hz) with rectified envelope in red. Inset shows expanded filtered traces from four electrodes within shaded yellow box, revealing consistent phase shifts (scale bar = 150 ms). **(C)** Modulation index extracted from the distribution of significant propagation angles from sample highly modulated electrode cluster (left) and minimally modulated electrode cluster (right). Dashed green line indicates the mean of the significant propagation angles across all the electrode clusters within the subdural grid (global mean) and dashed red line indicates the mean of the significant propagation angles in the individual electrode cluster (local mean). ‘a’ and ‘b’ represent the measures used to calculate modulation index (refer to ‘Materials and methods’ section). **(D)** Modulation index across a sample subdural grid; warm colours represent high modulation index. Red shaded box shows region displaying maximal IED-spindle coupling. **(E)** Polar plots demonstrating the propagation directions for the electrode clusters shown in **(C)** (left). Directions of preferred spindle travelling for all electrode clusters across a sample subdural grid are shown (right); note that the majority of clusters have two preferred directions of travel (blue and black arrows). **(F)** The majority of electrodes expressing spindles coupled to IEDs fall within the zone of maximal travelling modulation index (green circles). Red circles show the percentage of high modulation index electrodes outside of the IED-spindle coupling zone.

a coupled spindle oscillation. We demonstrated that spindles occur within a well-defined time interval after IEDs in humans, and that IEDs can drive cortical neural spiking at monosynaptic latencies in animals (Gelinas *et al.*, 2016). These characteristics suggest that pathological neural firing conveyed through synaptic interactions initiate IED-spindle coupling. However, IED-related neural firing could be conveyed to cortex via cortico-cortical or thalamocortical synapses (Alarcon *et al.*, 1997; Bourien *et al.*, 2005), and subsequent expression of spindles should recruit thalamocortical circuits (Steriade *et al.*, 1993). The similarity in the duration, frequency, and amplitude between coupled and uncoupled spindles supports the same basic neural substrate in their generation.

Insight into the pathways that support IED-spindle coupling can be gained by examining the anatomical relationship between pairs of regions that demonstrate these interactions. We were optimally positioned to assess these relationships due to the broad cortical electrode coverage in each patient, reducing bias associated with restricted sampling of neural signals. Pairs were located on average >6 cm apart (substantially larger than the width of a gyrus) (Thompson *et al.*, 1996) and typically consisted of two distinct brain regions based on cortical parcellation.

Thus, IED-spindle coupling in the human brain involves predominantly medium to long-range, rather than local, connections.

IED-spindle interactions were consistent with white matter connectivity patterns (Hagmann *et al.*, 2008; Jung *et al.*, 2017). There were prominent interactions between limbic/temporo-polar cortex and ventrolateral frontal cortex (Sedat and Duvernoy, 1990), as well as between lateral temporal, dorsolateral prefrontal, and parietal cortices (Schmahmann *et al.*, 2007), in keeping with tractography-defined networks (Dosenbach *et al.*, 2007). However, the anatomical distribution of IED-spindle coupling was also highly individualized. Similar variability occurs in the propagation of seizures and IEDs across patients with anatomically comparable epileptogenic lesions (Alarcon *et al.*, 1997; Proix *et al.*, 2017), and even in resting state functional connectivity across normal subjects (Mueller *et al.*, 2013).

Another factor that predicted IED-spindle coupling was the location of the epileptic network. Spindles coupled to IEDs were consistently observed in brain regions that did not generate IEDs and seizures. These regions were also unlikely to be recruited into early stages of seizure propagation. Therefore, expression of spindles temporally locked

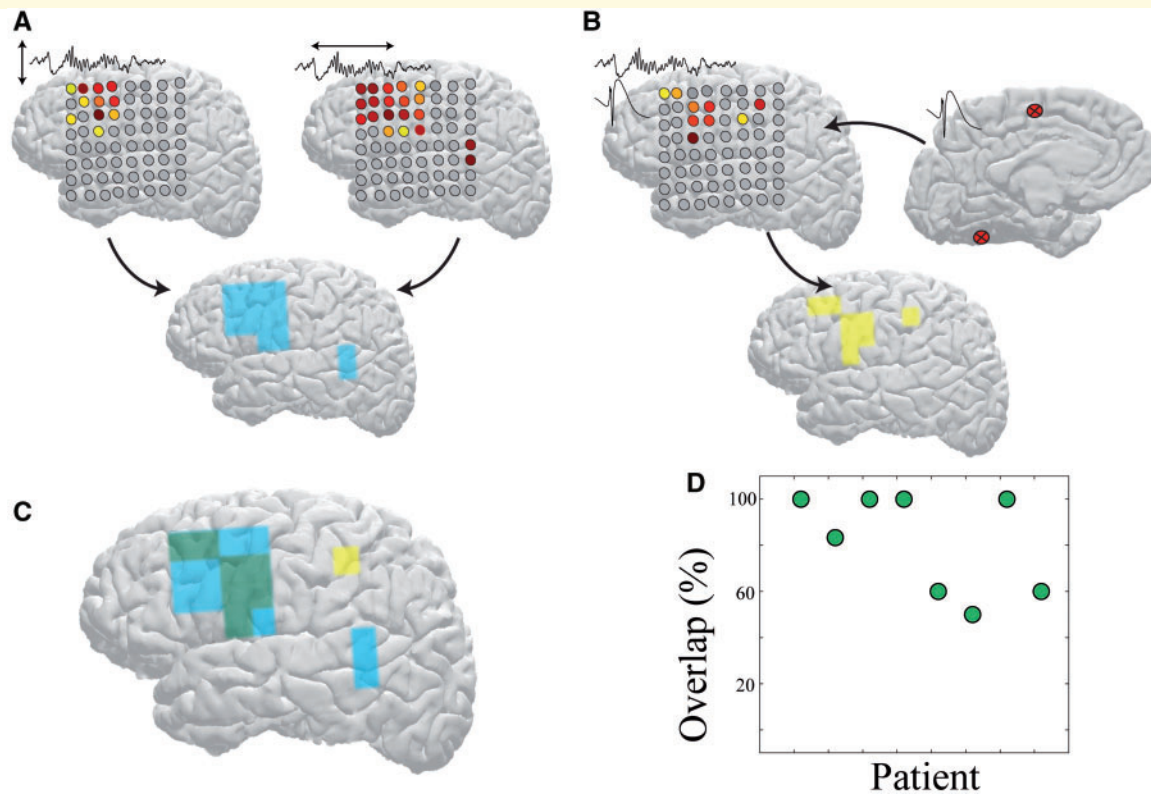


**Figure 6** Maximal spindle spatial extent and travelling predict brain regions influenced by IEDs. **(A)** Region of maximal spindle spatial extent (*left*) and maximal spindle travelling modulation index (*right*) obtained by watershed analysis of a sample patient's subdural grid. The regions representing the union between these measures are identified in blue (*bottom*). **(B)** Regions of significant spindle coupling (*left*) to IEDs generated at regions marked on the *right* for the same patient as in **A**. Regions of IED-spindle coupling are identified in yellow (*bottom*). **(C)** Overlap between regions of maximally extensive propagating spindles and regions expressing spindles coupled to IEDs (green). **(D)** Percentage of overlap between regions of maximally extensive propagating spindles and regions expressing spindles coupled to IEDs across all patients with > 20 significant IED-spindle pairs ( $n = 8$ ).

to IEDs likely reflects a directional interaction from the epileptic to the non-epileptic zone. The brain regions outside of the active ictal area during a seizure (Englot *et al.*, 2008; Schevon *et al.*, 2012) or immediately surrounding an IED focus (Serafini and Loeb, 2015) display neural firing and oscillations suggestive of increased inhibition. IED-spindle coupling in rats is associated with a strong inhibition of neural firing for hundreds of milliseconds prior to the start of the spindle oscillation (Gelinis *et al.*, 2016). Regions of IED-spindle coupling 'surround' the epileptic network, suggesting that these areas receive synaptic activity generated by IEDs, but can mount an inhibitory response that prevents IED propagation.

Cross-correlation and coherence analysis of spindles in our patients supports the strong local expression patterns of these oscillations (Caderas *et al.*, 1982; Nishida and Walker, 2007; Dehghani *et al.*, 2010; Andrillon *et al.*, 2011; Halassa *et al.*, 2011), though some spindles have a more global distribution (Muller *et al.*, 2016). We also found evidence that regionally restricted spindles can travel across the cortical surface, consistent with travelling waves in other frequencies in the awake human brain

(Takahashi *et al.*, 2011; Zhang *et al.*, 2018). We found that spindles in brain regions expressing IED-spindle coupling have a larger spatial extent and higher propensity to travel compared to those in brain regions without IED-coordinated activity. Increased frequency-specific coherence between functionally-related brain regions and travelling waves correlate with successful task-based information processing (Hipp *et al.*, 2011; Samaha and Postle, 2015; Rohenkohl *et al.*, 2018; Zhang *et al.*, 2018). In contrast, lack of functionally segregated network activity is associated with immature neural networks and impaired neurocognitive performance (Dosenbach *et al.*, 2010; Ibrahim *et al.*, 2014). IED-induced increases to coherence and traveling of spindles could disrupt the spatiotemporal specificity of these oscillations and impair functional neural computation.

Focal epilepsy is associated with brain dysfunction that extends beyond the epileptic network (Bettus *et al.*, 2011; Englot *et al.*, 2016; Lagarde *et al.*, 2018; Tong *et al.*, 2019). This dysfunction may contribute to cognitive impairments in these patients (Hermann *et al.*, 2006) and prime the brain for further spread of the epileptic network

(Sato *et al.*, 1998; Velisek and Moshe, 2003), but lack of mechanistic understanding limits approaches to treatment. Our results identify IED-spindle coupling as a consistent but individualized pattern of dynamically coordinated interactions between the epileptic network and surrounding brain regions. Brain regions that exhibit this coupling also display altered capacity for oscillatory expression and propagation that persists beyond the epochs of coupling, allowing them to be identified even in the absence of IEDs. IED-spindle coupling may therefore play a role in establishing the altered global connectivity observed in patients with focal epilepsy. Detection and manipulation of these patterns of coordinated brain activity (Maingret *et al.*, 2016) will permit causal testing of this hypothesis and may present new opportunities for therapies to address distributed network dysfunction in epilepsy.

## Acknowledgements

We thank B. Mahmood for help with accessing relevant data. Thanks also to H.X. Wang for providing the MRI-based electrode localizations for these data.

## Funding

This work was supported by a Taking Flight award from CURE (Citizens United for Research in Epilepsy), Finding A Cure for Epilepsy and Seizures (FACES), as well as the Department of Neurology and Institute for Genomic Medicine at Columbia University Irving Medical Center.

## Competing interests

The authors report no competing interests.

## Supplementary material

Supplementary material is available at *Brain* online.

## References

- Alarcon G, Garcia Seoane JJ, Binnie CD, Martin Miguel MC, Juler J, Polkey CE, et al. Origin and propagation of interictal discharges in the acute electrocorticogram. Implications for pathophysiology and surgical treatment of temporal lobe epilepsy. *Brain* 1997; 120 (Pt 12): 2259–82.
- Andrillon T, Nir Y, Staba RJ, Ferrarelli F, Cirelli C, Tononi G, et al. Sleep spindles in humans: insights from intracranial EEG and unit recordings. *J Neurosci* 2011; 31: 17821–34.
- Bartolomei F, Lagarde S, Wendling F, McGonigal A, Jirsa V, Guye M, et al. Defining epileptogenic networks: Contribution of SEEG and signal analysis. *Epilepsia* 2017; 58: 1131–47.
- Benchenane K, Peyrache A, Khamassi M, Tierney PL, Gioanni Y, Battaglia FP, et al. Coherent theta oscillations and reorganization of spike timing in the hippocampal–prefrontal network upon learning. *Neuron* 2010; 66: 921–36.
- Bettus G, Ranjeva JP, Wendling F, Benar CG, Confort-Gouny S, Regis J, et al. Interictal functional connectivity of human epileptic networks assessed by intracerebral EEG and BOLD signal fluctuations. *PLoS One* 2011; 6: e20071.
- Bourien J, Bartolomei F, Bellanger JJ, Gavaret M, Chauvel P, Wendling F. A method to identify reproducible subsets of co-activated structures during interictal spikes. Application to intracerebral EEG in temporal lobe epilepsy. *Clin Neurophysiol* 2005; 116: 443–55.
- Bragin A, Engel J Jr, Wilson CL, Fried I, Mathern GW. Hippocampal and entorhinal cortex high-frequency oscillations (100–500 Hz) in human epileptic brain and in kainic acid–treated rats with chronic seizures. *Epilepsia* 1999; 40: 127–37.
- Buzsaki G, Schomburg EW. What does gamma coherence tell us about inter-regional neural communication? *Nat Neurosci* 2015; 18: 484–9.
- Caderas M, Niedermeyer E, Uematsu S, Long DM, Nastalski J. Sleep spindles recorded from deep cerebral structures in man. *Clin Electroencephalogr* 1982; 13: 216–225.
- Cole S and Voytek B. Cycle-by-cycle analysis of neural oscillations. *bioRxiv* 2018; 302000.
- de Curtis M, Avoli M. Initiation, Propagation, and Termination of Partial (Focal) Seizures. *Cold Spring Harb Perspect Med* 2015; 5: a022368.
- Dehghani N, Cash SS, Chen CC, Hagler DJ, Jr., Huang M, Dale AM, et al. Divergent cortical generators of MEG and EEG during human sleep spindles suggested by distributed source modeling. *PLoS One* 2010; 5: e11454.
- Desikan RS, Segonne F, Fischl B, Quinn BT, Dickerson BC, Blacker D, et al. An automated labeling system for subdividing the human cerebral cortex on MRI scans into gyral based regions of interest. *Neuroimage* 2006; 31: 968–80.
- Diekelmann S, Born J. The memory function of sleep. *Nat Rev Neurosci* 2010; 11: 114–26.
- Dosenbach NU, Fair DA, Miezin FM, Cohen AL, Wenger KK, Dosenbach RA, et al. Distinct brain networks for adaptive and stable task control in humans. *Proc Natl Acad Sci USA* 2007; 104: 11073–8.
- Dosenbach NU, Nardos B, Cohen AL, Fair DA, Power JD, Church JA, et al. Prediction of individual brain maturity using fMRI. *Science* 2010; 329: 1358–61.
- Englot DJ, Konrad PE, Morgan VL. Regional and global connectivity disturbances in focal epilepsy, related neurocognitive sequelae, and potential mechanistic underpinnings. *Epilepsia* 2016; 57: 1546–57.
- Englot DJ, Mishra AM, Mansuripur PK, Herman P, Hyder F, Blumenfeld H. Remote effects of focal hippocampal seizures on the rat neocortex. *J Neurosci* 2008; 28: 9066–81.
- Frauscher B, von Ellenrieder N, Ferrari-Marinho T, Avoli M, Dubeau F, Gotman J. Facilitation of epileptic activity during sleep is mediated by high amplitude slow waves. *Brain* 2015; 138: 1629–41.
- Fries P. A mechanism for cognitive dynamics: neuronal communication through neuronal coherence. *Trends Cogn Sci* 2005; 9: 474–80.
- Gais S, Molle M, Helms K, Born J. Learning-dependent increases in sleep spindle density. *J Neurosci* 2002; 22: 6830–4.
- Gelinas JN, Khodagholy D, Thesen T, Devinsky O, Buzsaki G. Interictal epileptiform discharges induce hippocampal-cortical coupling in temporal lobe epilepsy. *Nat Med* 2016; 22: 641–8.
- Hagmann P, Cammoun L, Gigandet X, Meuli R, Honey CJ, Wedeen VJ, et al. Mapping the structural core of human cerebral cortex. *PLoS Biol* 2008; 6: e159.
- Halassa MM, Siegle JH, Ritt JT, Ting JT, Feng G, Moore CI. Selective optical drive of thalamic reticular nucleus generates thalamic bursts and cortical spindles. *Nat Neurosci* 2011; 14: 1118–20.
- Hermann BP, Seidenberg M, Dow C, Jones J, Rutecki P, Bhattacharya A, et al. Cognitive prognosis in chronic temporal lobe epilepsy. *Ann Neurol* 2006; 60: 80–7.

- Hipp JF, Engel AK, Siegel M. Oscillatory synchronization in large-scale cortical networks predicts perception. *Neuron* 2011; 69: 387–96.
- Ibrahim GM, Cassel D, Morgan BR, Smith ML, Otsubo H, Ochi A, et al. Resilience of developing brain networks to interictal epileptiform discharges is associated with cognitive outcome. *Brain* 2014; 137: 2690–702.
- Igarashi KM, Lu L, Colgin LL, Moser MB, Moser EI. Coordination of entorhinal-hippocampal ensemble activity during associative learning. *Nature* 2014; 510: 143–7.
- Johnson LA, Euston DR, Tatsuno M, McNaughton BL. Stored-trace reactivation in rat prefrontal cortex is correlated with down-to-up state fluctuation density. *J Neurosci* 2010; 30: 2650–61.
- Jung J, Cloutman LL, Binney RJ, Lambon Ralph MA. The structural connectivity of higher order association cortices reflects human functional brain networks. *Cortex* 2017; 97: 221–39.
- Lagarde S, Roehri N, Lambert I, Trebuchon A, McGonigal A, Carron R, et al. Interictal stereotactic-EEG functional connectivity in refractory focal epilepsies. *Brain* 2018; 141: 2966–80.
- Maingret N, Girardeau G, Todorova R, Goutierre M, Zugaro M. Hippocampo-cortical coupling mediates memory consolidation during sleep. *Nat Neurosci* 2016; 19: 959–64.
- Massimini M, Ferrarelli F, Esser SK, Riedner BA, Huber R, Murphy M, et al. Triggering sleep slow waves by transcranial magnetic stimulation. *Proc Natl Acad Sci USA* 2007; 104: 8496–501.
- Mueller S, Wang D, Fox MD, Yeo BT, Sepulcre J, Sabuncu MR, et al. Individual variability in functional connectivity architecture of the human brain. *Neuron* 2013; 77: 586–95.
- Muller L, Piantoni G, Koller D, Cash SS, Halgren E, Sejnowski TJ. Rotating waves during human sleep spindles organize global patterns of activity that repeat precisely through the night. *Elife* 2016; 5: e17267.
- Nir Y, Staba RJ, Andrillon T, Vyazovskiy VV, Cirelli C, Fried I, et al. Regional slow waves and spindles in human sleep. *Neuron* 2011; 70: 153–69.
- Nishida M, Walker MP. Daytime naps, motor memory consolidation and regionally specific sleep spindles. *PLoS One* 2007; 2: e341.
- Proix T, Bartolomei F, Guye M, Jirsa VK. Individual brain structure and modelling predict seizure propagation. *Brain* 2017; 140: 641–54.
- Rohenkohl G, Bosman CA, Fries P. Gamma synchronization between V1 and V4 improves behavioral performance. *Neuron* 2018; 100: 953–63.e953.
- Rosenow F, Luders H. Presurgical evaluation of epilepsy. *Brain* 2001; 124: 1683–700.
- Rubino D, Robbins KA and Hatsopoulos NG. Propagating waves mediate information transfer in the motor cortex. *Nat Neurosci* 2006; 9: 1549–57.
- Samaha J, Postle BR. The speed of alpha-band oscillations predicts the temporal resolution of visual perception. *Curr Biol* 2015; 25: 2985–90.
- Sato T, Yamada N, Morimoto K, Uemura S, Kuroda S. A behavioral and immunohistochemical study on the development of perirhinal cortical kindling: a comparison with other types of limbic kindling. *Brain Res* 1998; 811: 122–32.
- Sawangjit A, Oyanedel CN, Niethard N, Salazar C, Born J, Inostroza M. The hippocampus is crucial for forming non-hippocampal long-term memory during sleep. *Nature* 2018; 564: 109–13.
- Schevon CA, Weiss SA, McKhann G Jr, Goodman RR, Yuste R, Emerson RG, et al. Evidence of an inhibitory restraint of seizure activity in humans. *Nat Commun* 2012; 3: 1060.
- Schmahmann JD, Pandya DN, Wang R, Dai G, D’Arceuil HE, de Crespigny AJ, et al. Association fibre pathways of the brain: parallel observations from diffusion spectrum imaging and autoradiography. *Brain* 2007; 130: 630–53.
- Sedat J, Duvernoy H. Anatomical study of the temporal lobe. Correlations with nuclear magnetic resonance. *J Neuroradiol* 1990; 17: 26–49.
- Serafini R, Loeb JA. Enhanced slow waves at the periphery of human epileptic foci. *Clin Neurophysiol* 2015; 126: 1117–23.
- Siapas AG, Wilson MA. Coordinated interactions between hippocampal ripples and cortical spindles during slow-wave sleep. *Neuron* 1998; 21: 1123–8.
- Stark E, Abeles M. Unbiased estimation of precise temporal correlations between spike trains. *J Neurosci Methods* 2009; 179: 90–100.
- Steriade M, McCormick DA, Sejnowski TJ. Thalamocortical oscillations in the sleeping and aroused brain. *Science* 1993; 262: 679–85.
- Takahashi K, Saleh M, Penn RD, Hatsopoulos NG. Propagating waves in human motor cortex. *Front Hum Neurosci* 2011; 5: 40.
- Thompson PM, Schwartz C, Lin RT, Khan AA, Toga AW. Three-dimensional statistical analysis of sulcal variability in the human brain. *J Neurosci* 1996; 16: 4261–74.
- Tong X, An D, Xiao F, Lei D, Niu R, Li W, et al. Real-time effects of interictal spikes on hippocampus and amygdala functional connectivity in unilateral temporal lobe epilepsy: an EEG-fMRI study. *Epilepsia* 2019; 60: 246–54.
- Ujma PP, Halasz P, Kelemen A, Fabo D, Eross L. Epileptic interictal discharges are more frequent during NREM slow wave downstates. *Neurosci Lett* 2017; 658: 37–42.
- Velisek L, Moshe SL. Temporal lobe epileptogenesis and epilepsy in the developing brain: bridging the gap between the laboratory and the clinic. Progression, but in what direction? *Epilepsia* 2003; 44 (Suppl 12): 51–9.
- Vyazovskiy VV, Faraguna U, Cirelli C, Tononi G. Triggering slow waves during NREM sleep in the rat by intracortical electrical stimulation: effects of sleep/wake history and background activity. *J Neurophysiol* 2009; 101: 1921–31.
- Wierzynski CM, Lubenov EV, Gu M, Siapas AG. State-dependent spike-timing relationships between hippocampal and prefrontal circuits during sleep. *Neuron* 2009; 61: 587–96.
- Yang AI, Wang X, Doyle WK, Halgren E, Carlson C, Belcher TL, et al. Localization of dense intracranial electrode arrays using magnetic resonance imaging. *Neuroimage* 2012; 63: 157–65.
- Zhang H, Watrous AJ, Patel A, Jacobs J. Theta and alpha oscillations are traveling waves in the human neocortex. *Neuron* 2018; 98: 1269–81.e1264.